Synthesis, spectroscopic and electrochemical properties of manganese, nickel and iron octakis-(2-diethylaminoethanethiol)-phthalocyanine

Akinbulu Isaac Adebayo and Tebello Nyokong*

[a]Department of Chemistry, Rhodes University, Grahamstown 6140, South Africa

Abstract

The syntheses, spectroscopic and electrochemical properties of manganese (3), nickel (4) and iron (5) phthalocyanine complexes, octa-substituted at the peripheral positions with diethlyaminoethanethiol substituent, are reported. The electrochemistry of these complexes and the corresponding cobalt complex (6) are reported. Complex 3 showed two reversible reduction couples attributed to the $Mn^{III}Pc^{-2}/Mn^{II}Pc^{-2}$ ($E_{½}$ = −0.12 V versus Ag|AgCl) and $Mn^{II}Pc^{-2}/Mn^{II}Pc^{-3}$ ($E_{½}$ = −0.82 V versus Ag|AgCl) species. Two ring-based reduction couples were also observed for complex 4. Two reduction couples, assigned to the $Fe^{II}Pc^{-2}/Fe^{I}Pc^{-2}$ ($E_{½}$ = −0.35 V versus Ag|AgCl) and $Fe^{I}Pc^{-2}/Fe^{I}Pc^{-3}$ ($E_{½}$ = −0.96 V versus Ag|AgCl) species, and an oxidation couple, attributed to $Fe^{III}Pc^{-2}/Fe^{II}Pc^{-2}$ ($E_{½}$ = 0.26 V versus Ag|AgCl) species, were observed. For complex 6, two reductions and one oxidation were also observed with the potential range of 1.2 to −1.8 V versus Ag|AgCl Spectroelectrochemical studies were used to confirm some of the assigned processes.

Graphical abstract

Manganese (3), nickel (4) and iron (5) phthalocyanine complexes, octa-substituted at the peripheral positions with diethlyaminoethanethiol substituents show that the central metal plans a significant role in the aggregation behavior, with Mn phthalocyanine derivatives showing the presence of μ oxo dimers.

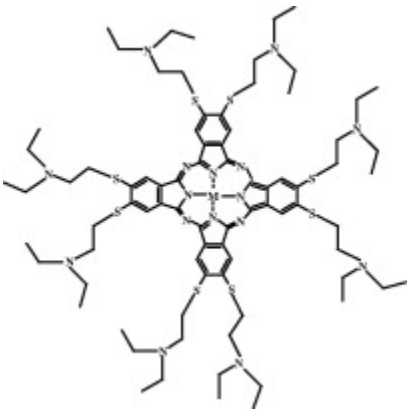

1. Introduction

Metallophthalocyanine (MPc) complexes are being extensively researched because of their diverse applications. These include their uses in electronic devices, as gas sensors, as photosensitizers, in non-linear optics, in electrochromic devices and in Langmuir–Blodgett films [1] and [2]. The desired physical, chemical, electronic, electrochemical and other properties of these macrocycles, which are key to their suitability for the above applications, can be obtained by careful selection of the central metals, type and position (peripheral and non-peripheral) of the substituents. ZnPc and CoPc complexes containing diethylaminoethanethiol substituents have recently been reported [3] and [4]. However, the electrochemical characterization of the CoPc complex has not been reported, and is reported here for the first time. In the current work, we report on the synthesis, spectroscopic and electrochemical properties of new MnPc, FePc and NiPc complexes octa-substituted at the peripheral positions with bulky diethylaminoethanethiol (Scheme 1). Co, Fe and Mn central metals are electroactive in MPc complexes, hence are chosen in this work. The electrochemistry of MPc complexes of Mn, Ni, Fe and Co, containing diethylaminoethanethiol, is reported for the first time. This ligand contains nitrogen and sulfur atoms, giving phthalocyanine complexes which may readily be polymerized or form self-assembled monolayer on gold electrodes. MnPc derivatives show interesting electrochemical behavior with oxidation states of the central Mn ion ranging from Mn^{I} to Mn^{IV} [5], [6], [7], [8] and [9]. In addition, the first reduction in $Mn^{II}Pc^{-2}$ complexes has been a subject of some controversy, with some reports proposing ring reduction to the $Mn^{II}Pc^{-3}$ species and others suggesting metal reduction to the $Mn^{I}Pc^{-2}$ species [5] and [10].

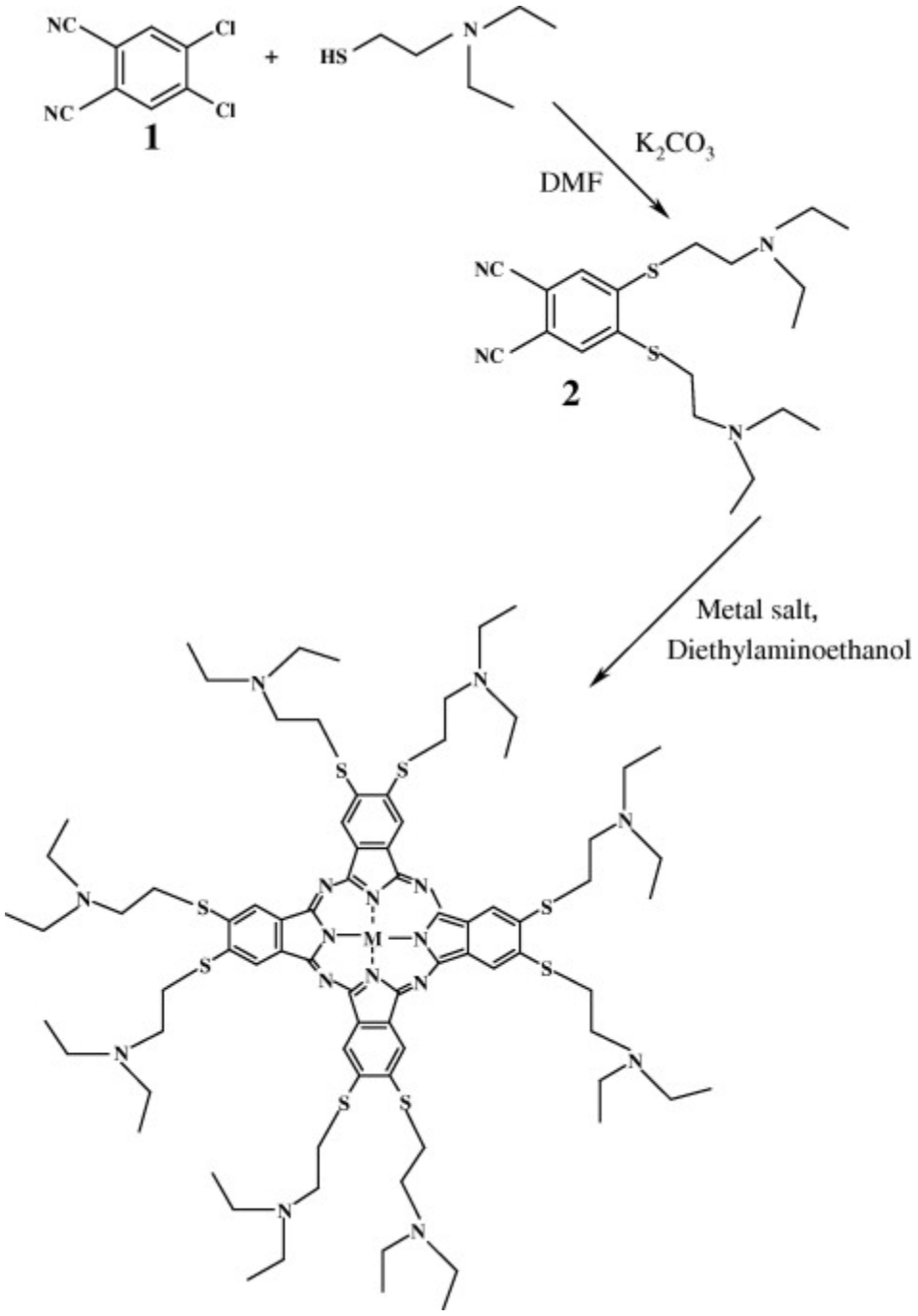

Scheme 1. Synthetic pathway for octakis-(2-diethylaminoethanethiol)-phthalocyanine. M = MnAc (3), Ni (4), Fe (5) and Co (6) [4].

Electrochemistry of alkylthio or arylthio substituted MPc complexes is often different from that of other substituted MPc complexes. For example, irreversible ring-based processes coupled with chemical reactions and adsorption of the reduction products, overlap of reduction couples to form one peak, multi-electron processes and degradation have been reported [11], [12], [13], [14], [15] and [16].

2. Experimental

2.1. Materials

Potassium carbonate, manganese acetate, cobalt chloride, iron(II) chloride tetrahydrate (containing less than 0.2% iron(III) salt), nickel(II) chloride hexahydrate, 2-(diethylaminoethanethiol) hydrochloride and 2-diethylaminoethanol were obtained from Sigma–Aldrich. Anhydrous form of nickel(II) chloride and iron(II) chloride were obtained by heating the hydrated form in an oven. Tetrabutylammonium tetrafluoroborate ($TBABF_4$) (Aldrich) was used as the electrolyte for electrochemical experiments. All solvents were dried and distilled before use. Aluminum oxide, WN-3: neutral, for column chromatography, was purchased from Sigma–Aldrich. Tetrahydrofuran (THF), dimethylformamide (DMF) and dichloromethane (DCM) were obtained from Merck. The synthesis of cobalt octakis-(2-diethylaminoethanethiol)-phthalocyanine (6) has been reported before [4].

2.2. Electrochemical studies

All electrochemical experiments were performed using Autolab potentiostat PGSTAT 302 (Eco Chemie, Utrecht, The Netherlands) driven by the general purpose Electrochemical System data processing software (GPES, software version 4.9). Square wave voltammetric analysis was carried out at a frequency of 10 Hz, amplitude; 50 mV and step potential; 5 mV. A conventional three-electrode system was used. The working electrode was a bare glassy carbon electrode (GCE), Ag|AgCl wire and platinum wire were used as the pseudo reference and auxiliary electrodes respectively. The potential response of the Ag|AgCl pseudo-reference electrode was less than the Ag|AgCl (3 M KCl) by 0.015 ± 0.003 V. Prior to use, the working electrode surface was polished with alumina on a Buehler felt pad and rinsed with excess millipore water. All electrochemical experiments were performed in freshly distilled dry DMF or DCM containing $TBABF_4$ as supporting electrolyte.

Spectroelectrochemical data were obtained using a home-made optically transparent thin-layer electrochemical (OTTLE) cell which was connected to a Bioanalytical Systems (BAS) CV 27 voltammograph.

2.3. Equipment

UV/Vis spectra were recorded on Cary 500 UV/Vis/NIR spectrophotometer. IR (KBr disks) was recorded on Bruker Vertex 70-Ram II spectrophotometer. Elemental analysis was performed using Vario Elementar Microcube EL111. ^{1}H nuclear magnetic resonance (^{1}H NMR, 400 MHz) was obtained in $CDCl_3$ using Bruker EMX 400 NMR spectrometer.

2.4. Synthesis

2.4.1. 1,2-Bis-(diethylaminoethanethiol)-4, 5-dicyanobenzene (2)

1,2-Dichloro-4,5-dicyanobenzene (1) was synthesised according to reported procedures [17]. 1,2-Bis-(2-diethylaminoethanethiol)-4,5-dicyanobenzene (2) was also synthesised according to literature procedure [4], with slight modification as follows: compound 1 (2.32 g, 11.75 mmol) was dissolved in anhydrous DMF (100 ml) under nitrogen and 2-diethylaminoethanethiol hydrochloride (6 g, 35.34 mmol) was added. After stirring for 10 min, finely ground anhydrous K_2CO_3 (19.5 g, 141.36 mmol) was added in portions over 2 h with stirring. The reaction mixture was stirred at room temperature for 48 h under nitrogen. Then the solution was poured into ice water (600 g). The precipitate was filtered off, washed with water, until the filtrate was neutral. The product was then dried in air. Yield: 3.61 g (80%). IR (KBr) ν_{max}/cm^{-1}: 3075, 2970–2812, 2229, 1562, 1459, 1382, 1343, 1275, 1200, 1113, 1066, 991, 733, 529. ^{1}H NMR ($CDCl_3$) δ = 7.54 (s, 2H,Ar–H), 3.12–3.08 (t, 4H, SCH_2), 2.80–2.77 (t, 4H, NCH_2), 2.61–2.55 (qnt, 8H, CH_2C), 1.05–1.01 (t, 12H, CH_3) ppm.

2.4.2. Manganese(III)acetate (3), nickel (4) and iron (5) octakis-(2-diethylaminoethanethiol)-phthalocyanine

Manganese(III)acetate (3), nickel (4) and iron (5) octakis-(2-diethylaminoethanethiol)-phthalocyanine were synthesised according to the procedure recently reported [3] and [4] with some modifications. A mixture of compound 2 (0.6 g, 1.54 mmol), manganese acetate (0.066 g, 0.38 mmol) or nickel(II) chloride (0.049 g, 0.38 mmol) or iron(II) chloride (0.049 g, 0.38 mmol) and 2-(dimethylaminoethanol) (1.2 ml)

was refluxed for 12 h under nitrogen. After cooling to room temperature, the mixture was treated with excess MeOH: H_2O (1:1 ml) in order to precipitate the products. The products were filtered and dried in air. The products were then purified using column chromatography with neutral alumina as column material and DCM/methanol (20:1) as eluent.

2.4.2.1. Complex 3

Yield: 0.54 g (86.72%) (*Anal.* Calc. for $C_{80}H_{120}N_{16}S_8MnOAc{\cdot}CH_2Cl_2$: C, 58.51; H, 7.34; N, 13.16. Found: C, 57.11; H, 6.72; N, 12.63%); UV–Vis (THF): λ_{max} (nm) (log ε): 353(4.6), 423(4.5), 465(4.5), 503(4.4), 676(4.3), 750(5.0); IR (KBr) ν_{max}/cm^{-1}; 2966–2805 (CH_2), 1413, 1377, 1327, 1070, 781, 744, 705, 606.

2.4.2.2. Complex 4

Yield: 0.15 g (24.03%) (*Anal.* Calc. for $C_{80}H_{120}N_{16}S_8Ni{\cdot}CH_2Cl_2$: C, 56.97; H, 7.15; N, 13.13. Found: C, 56.35; H, 6.93; N, 13.17%); UV–Vis (THF): λ_{max} (nm) (log ε): 425(4.4), 695(4.8); IR (KBr) ν_{max}/cm^{-1} 2970–2802 (CH_2), 1410, 1367, 1307, 1080, 786, 754, 725, 686.

2.4.2.3. Complex 5

Yield: 0.28 g (44.94%) (*Anal.* Calc. for $C_{80}H_{120}N_{16}S_8Fe{\cdot}2CH_2Cl_2$: C, 55.07; H, 6.93; N, 12.52. Found: C, 54.71; H, 6.71; N, 12.34%); UV–Vis (DMF): λ_{max} (nm) (log ε): 360(4.4), 451(3.9), 621(3.7), 657(3.9), 686(4.1), 746(3.8); IR (KBr) ν_{max}/cm^{-1} 2972–2805 (CH_2), 1412, 1357, 1317, 1080, 789, 758, 735, 688.

3. Results and discussion

3.1. Synthesis and characterization

3.1.1. Synthesis

Scheme 1 shows the synthetic route involved in the formation of complexes 3, 4 and 5. The phthalonitrile, compound 2, was obtained via a based-catalyzed (K_2CO_3) nucleophilic aromatic substitution reaction, with the 2-diethylaminoethanethiol acting as the nucleophile. Cyclotetramerization of compound 2 to form the corresponding MPc occurred in the presence of the desired metal salt; $Mn(CH_3COO)_2$, $NiCl_2$ and $FeCl_2$ for complexes 3, 4 and 5, respectively. Purification of these complexes was achieved by column

chromatography on alumina. Complex 3 was soluble in solvents such as THF, DCM and DMF while complex 4 dissolved in THF and DCM. Complex 5 was soluble in DMF and DCM but insoluble in THF.

These complexes were characterized by IR and UV–Vis spectroscopies as well as elemental analysis. The results obtained were consistent with the predicted structures shown in Scheme 1. The formation of complexes 3, 4 and 5 was confirmed by the disappearance of the sharp C≡N vibration at 2229 cm^{-1} of 2.

3.1.2. Spectroscopic characterization

All the complexes exhibited spectral properties characteristic of metallophthalocyanine (MPc). Complex 3 showed characteristic Q-band absorption, in THF, at 750 nm, Fig. 1. The absorption in the 450 nm region is usually associated with charge transfer in MnPc [10]. Complex 4 showed considerable aggregation in THF, with the peak at 694 nm attributed to the monomer while that at 633 nm is due to the aggregate, Fig. 1. Extensive aggregation of NiPc derivatives has been observed before [18]. Fig. 1 shows that the Q-band due to complex 3 is appreciably red-shifted compared to complex 4. This observation is characteristic of MnPc complexes [10].

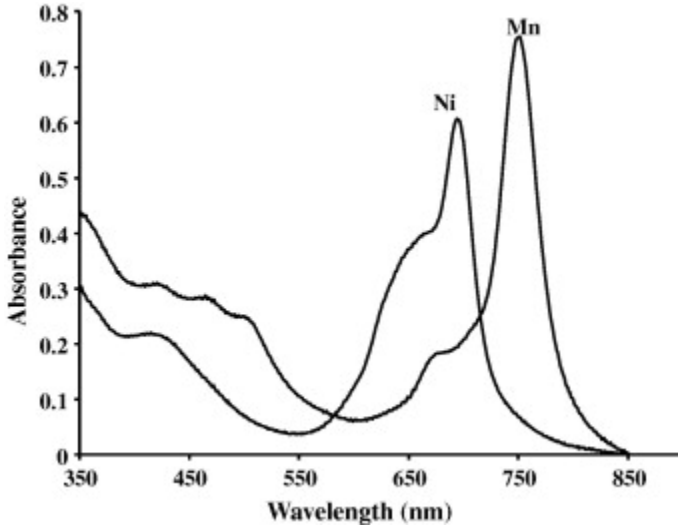

Fig. 1. UV–Vis spectra of 6.7×10^{-6} M of complex 3 (Mn) and complex 4 (Ni) in THF.

Fig. 2a shows the effect of increasing concentration (3.3×10^{-6}–8.8×10^{-6} M) on the spectra of complex 3. Inset in Fig. 2a is a linear plot of absorbance, due to the Q-band (750 nm), against concentration of complex 3. There was no evidence of aggregation in Fig. 2a and Beer's law was obeyed for concentrations less than 1×10^{-5}. Fig. 2b shows the effect of changing concentration (1.7×10^{-6}–1.02×10^{-5}M) on the spectra of complex 4. The intensities of both the monomeric (694 nm) and dimeric peaks (633 nm) decreased with decreasing concentration. The Q-band due to the aggregate became less pronounced, compared to that due to the monomer, as concentration decreased, thus confirming the aggregated nature of the complex. Inset in Fig. 2b is the plot of absorbance, due to the Q-band at 694 nm, versus concentration. Even though the plot is almost linear at these concentrations, the UV–Vis spectra do give evidence of aggregation.

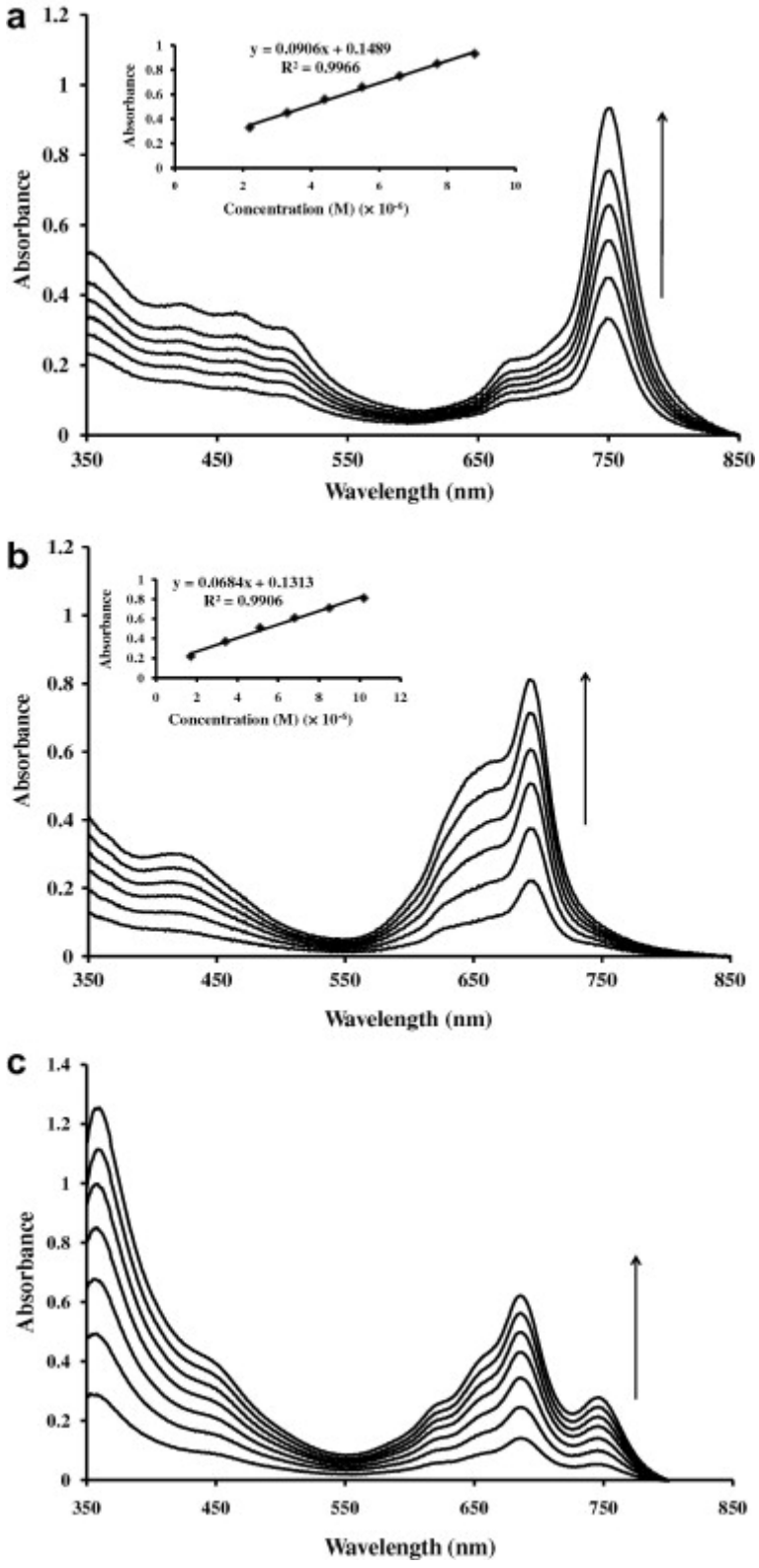
a
y = 0.0906x + 0.1489
R² = 0.9966
Absorbance
Concentration (M) (× 10⁻⁶)
Absorbance
Wavelength (nm)
b
y = 0.0684x + 0.1313
R² = 0.9906
Absorbance
Concentration (M) (× 10⁻⁶)
Absorbance
Wavelength (nm)
c
Absorbance
Wavelength (nm)

Fig. 2. Effect of changing concentration on the UV–Vis spectra of (a) complex 3 ($3.3–8.8 \times 10^{-6}$ M) in THF; (b) complex 4 (1.7×10^{-6}–1.02×10^{-5} M) in THF and (c) complex 5 (7.42×10^{-6}–5.2×10^{-5} M) in DMF.

Complex 5 (not soluble in THF) exhibited spectra (Fig. 2c) characteristic of stacked monomer in FePc complexes, which is normally observed at about 630 nm in DMF [19]. The UV/visible spectral analysis of FePc complexes has been a subject of extensive research due to the complexity and the wide variety of species that may be formed in solution. For example, perchlorinated iron(II) phthalocyanine dissolved in DMF is known [20] to react with oxygen, resulting in oxidation and formation of a μ-oxo species, $Pc^{-2}Fe^{III}–O–Fe^{III}Pc^{-2}$, which changes back to the original monomeric species upon reduction. In the present study, Fig. 2c, the spectra were obtained in freshly prepared DMF solutions which had been de-aerated, suggesting that the peak near 630 nm is not related to the μ-oxo species, but only to the presence of monomeric species as well as cofacially aggregated one. On dilution (5.2×10^{-5} M–7.42×10^{-6}), the peak near 630 nm decreased faster than the main peak at 686 nm. Aggregation (the presence of the band near 630 nm) was evident, even at concentration as low as 7.42×10^{-6} M, Fig. 2c. The split in the main Q-band suggests the presence of $Fe^{III}Pc$ species [10].

3.1.3. Voltammetric and spectroelectrochemical characterization

Voltammetric properties of complexes 3, 4, 5 and 6 are reported in this work. The peak potentials for the complexes are summarized in Table 1. In the current work, clearly defined reversible ring reductions were observed for all the complexes, but the reduction products get easily adsorbed on the electrode and the complexes degrade fast upon oxidation, especially the FePc derivative.

Table 1.

Electrochemical data of thiol substituted MnPc, FePc, NiPc and CoPc. Half-wave ($E_{1/2}$) and peak (E_p) potentials in V versus Ag|AgCl. Values were recorded in DMF containing $TBABF_4$ unless otherwise stated.

Complex	$M^{II}Pc^{-4}$ / $M^{II}Pc^{-3}$	$M^{I}_{2}Pc^{-3}/M^{I}Pc^{-}$	$M^{II}_{2}Pc^{-3}/M^{II}Pc^{-}$	$M^{II}Pc^{-2}$ / $M^{I}Pc^{-2}$	$M^{III}Pc^{-2}$ / $M^{II}Pc^{-2}$	$M^{II}Pc^{-1}$ / $M^{II}Pc^{-2}$	$M^{III}Pc^{-1}$ / $M^{III}Pc^{-2}$	Ref [c]
MnPc derivatives								
3			−0.82		−0.12		+0.78	TW
MnTMPyPc [a]					−0.057		+1.34	5
MnODMPc[a]			−1.24		−0.46		+ 0.75	12
MnTBMPc[a]			−0.98		−0.26		+0.83	28
4[a]	−0.69		−0.02			+0.92		
FePc derivatives								
5		−0.96		−0.35	+0.26		+0.87	
FeOBMPc[b]		−0.70		−0.26	+0.25		+0.60	29
FeTBMPc		−0.78		−0.37	+0.36		+0.70	26
FeTDMPc[a]		−0.84		−0.53	+0.62		+1.01	26
CoPc derivatives								
6		−1.40		−0.32	+0.80			
CoOBMPc[b]		−0.58		−0.096	+0.72		+1.16	29
CoTBMPc		−1.41		−0.38	+ 0.42		+0.89	26
CoTDMPc[a]				−0.46	+0.44		+0.66	26

TDMPc = tetra dodecylmercapto phthalocyanine, ODMPc = octa dodecylmercapto phthalocyanine

TBMPc = tetra benzylmercapto phthalocyanine, TMPyPc = tetra mercaptopyridine phthalocyanine.

[a] Values recorded in DCM, using $TBABF_4$.

[b] Electrolyte = tetrabutylammonium perchlorate.

[c] TW = this work.

3.1.3.1. Complex 3

Fig. 3 shows the cyclic and square wave (inset) voltammetry profiles of ~1 × 10^{-3} M of complex 3 in freshly distilled dimethyl formamide (DMF) containing 0.1 M $TBABF_4$ as supporting electrolyte. Three distinct processes, labeled I, II and III, can be identified. Redox couples II ($E_{1/2}$ = −0.12 V) and III ($E_{1/2}$ = −0.82 V) versus Ag|AgCl, have both anodic and cathodic components but with larger peak separation, ΔE (120 mV), than the expected 60 mV, thus suggesting slow electron transfer. These processes were quasi-reversible since ΔE value for ferrocene, at the same scan rate (100 mV versus Ag|AgCl), was 91 mV versus Ag|AgCl. The cathodic to anodic peak current ratio were near unity for both processes. Plots of peak current (I_p) versus square root of scan rate ($v^{1/2}$) (not shown) were linear for both processes, thus suggesting diffusion control. Redox couple II is assigned to $Mn^{III}Pc^{-2}/Mn^{II}Pc^{-2}$ while couple III is assigned to $Mn^{II}Pc^{-2}/Mn^{II}Pc^{-3}$ in comparison with literature [21], Table 1. Process I is irreversible (E_p = +0.78 V versus Ag|AgCl), it is assigned to ring oxidation, $Mn^{III}Pc^{-1}/Mn^{III}Pc^{-2}$ in comparison with literature, Table 1, [21]. The lack of reversibility of the oxidation processes is typical of thio substituted MPc complexes [14]. The redox processes and the number of electron transferred in each case were confirmed using spectroelectrochemical studies.

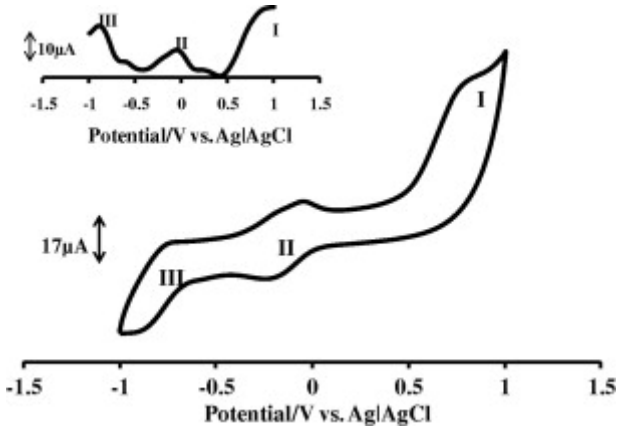

Fig. 3. Cyclic and square wave (inset) voltammograms of 10^{-3} M of complex 3 in freshly distilled DMF containing 0.1 M $TBABF_4$. Scan rate: 100 mVs^{-1}.

Spectroelectrochemical studies were carried out using optically transparent thin-layer electrode (OTTLE) cell. Fig. 4a shows the spectral changes observed on the application of potential of couple II (−0.12 V versus Ag|AgCl). The initial spectrum showed very pronounced peak at 653 nm with the main Q-band at 757 nm. The slight shift in the Q-band from 750 nm (Fig. 1) to 757 nm (Fig. 4a) is due to differences in solvents and the presence of electrolyte. The peak at 653 nm is characteristic of MnPc μ-oxo complexes [22]. This species is observed in DMF (Fig. 4a) but was not observed in THF (Fig. 1). The peak at 757 nm is due to $Mn^{III}Pc$ species. There is no $Mn^{II}Pc$ species before reduction. We used DMF for electrochemistry of complex 3 for comparative purposes with the other complexes under discussion in this work.

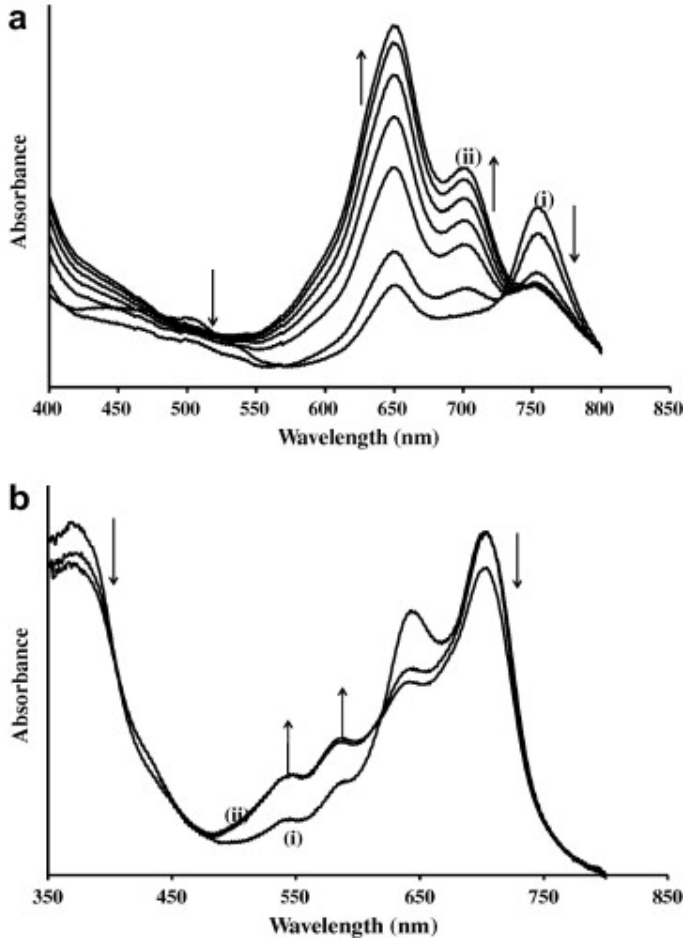

Fig. 4. UV–Vis spectral changes observed for complex 3 during controlled potential electrolysis at (a) −0.12 V (process II) and (b) −0.82 V (process III). (i) Spectra before electrolysis and (ii) spectra after electrolysis. The first spectrum in (b) is the same as the last spectrum in (b). Electrolyte = DMF containing 0.1 M $TBABF_4$.

The presence of the μ-oxo MnPc species was confirmed by monitoring the spectral transformations of complex 3 in DMF solution when not de-aerated and when de-aerated with dry N_2 gas. This was evident by the decrease of the peak at 653 nm on bubbling nitrogen. However attempts to exclude oxygen completely during spectroelectrochemical studies were unsuccessful. The cyclic and square wave voltammograms reported above (Fig. 3) were reported under an atmosphere of nitrogen hence are due to mainly the $Mn^{III}Pc$ species.

Upon reduction at potentials of processes II, there was a blue shift in the Q-band from 757 to 705 nm and the color of the complex changed from purple to green, a gradual disappearance of the charge transfer bands in the 500 nm region was also noticed, with an isobestic point at 736 nm. The isobestic point observed was not so clear, which suggests the presence of more than two species, thus confirming the presence of the μ-oxo complex with the starting $Mn^{III}Pc^{-2}$ species and the electro-generated species, $Mn^{II}Pc^{-2}$. The formation of the latter was accompanied by the formation of more μ-oxo MnPc species. The persistence of μ-oxo MnPc species has been observed for some MnPc complexes [23].

A shift in the position of the Q-band without a decrease in intensity is typical of metal-based electro reduction process, and a blue shift in the Q-band is usually associated with the reduction of $Mn^{III}Pc^{-2}$ to $Mn^{II}Pc^{-2}$ [10]. These spectra changes thus confirmed that redox couple II in Fig. 3 is due to the reduction of $Mn^{III}Pc^{-2}$ to $Mn^{II}Pc^{-2}$ (n was calculated to be approximately 1 using the Eq. (1),

(1)

$$Q=nFVC$$

where n, F, V and C are the number of electrons transferred, Faraday's constant, volume and concentration of the electroactive species, respectively.

Increase in intensity of the band at 653 nm confirmed the presence of the μ-oxo complex, as earlier discussed, together with the electro-generated $Mn^{II}Pc^{-2}$ species. This observation has been reported before [5], [22] and [23]. It was suggested that a form of equilibrium, as shown below, exists between MnPc species in DMF and in the presence of oxygen.

(2)

$$PcMn^{II}+O_2 \rightleftarrows PcMn^{III}(O_2)$$

(3)

$$PcMn^{III}(O_2)+PcMn^{II} \rightleftarrows PcMn^{III}–O_2–Mn^{III}Pc$$

(4)

$$PcMn^{III}–O_2–Mn^{III}Pc \rightleftarrows 2PcMn^{IV}O$$

(5)

$$2PcMn^{IV}O+2PcMn^{II} \rightleftarrows 2PcMn^{III}–O–Mn^{III}Pc$$

(6)

$$4PcMn^{II} + O_2 \rightarrow 2PcMn^{III}–O–Mn^{III}Pc \text{ (Net equation)}$$

Further reduction of complex 3, at the potentials of couple III, resulted in the spectral changes shown in Fig. 4b. A decrease in intensity of the new Q-band (705 nm) and emergence of new bands, with decreased intensities, at 543 and 590 nm are characteristic of ring-based redox process [24]. This observation confirmed that process III is a ring-based reduction, thus justifying the assignment of the couple to $Mn^{II}Pc^{-2}/Mn^{II}Pc^{-3}$ redox process. This supports the claim that first reduction in $Mn^{II}Pc^{-2}$ occur at the ring [25], although, other authors have reported metal reduction to the $Mn^{I}Pc^{-2}$ species [5] and [10]. Ring versus metal reduction in $Mn^{II}Pc$ complexes is highly dependent on the nature of substituents [5]. A decrease in intensity was also observed for the band (653 nm) associated with the μ-oxo complex.

Application of potential of process I resulted in the formation of a new less intense band at 509 nm, typical of ring oxidation in MPc [24], complicated by redox processes based on the ring substituents. Process I is thus assigned to ring oxidation, $Mn^{III}Pc^{-1}/Mn^{III}Pc^{-2}$.

3.1.3.2. Complex 4

Fig. 5 shows the cyclic and square wave (inset) voltammograms of 10^{-3} M complex 4 in a mixture of freshly distilled DCM and DMF (2:1) containing 0.1 M $TBABF_4$ as supporting electrolyte. This mixture was used because of the difficulty of obtaining a clearly defined cyclic voltammogram of the complex in DCM and the insoluble nature of the complex in DMF alone. Three processes can be observed: processes

I (E_p = +0.92 V), II ($E_{1/2}$ = −0.02 V) and III ($E_{1/2}$ = −0.69 V). All redox processes are assigned to the ring since only ring reduction or oxidation has been documented for NiPc complexes in solution [10]. The first reduction process is observed at less negative potentials than has been reported [18] for NiPc complexes, probably due to the presence of sulfur and nitrogen in the ring substituents which will make the ring easier to oxidize. Couple II and III were reversible, while process I was irreversible. Due to the aggregated nature of the complex, it was not possible to do reliable spectroelectrochemical studies, however only ring-based redox processes occur for NiPc derivatives.

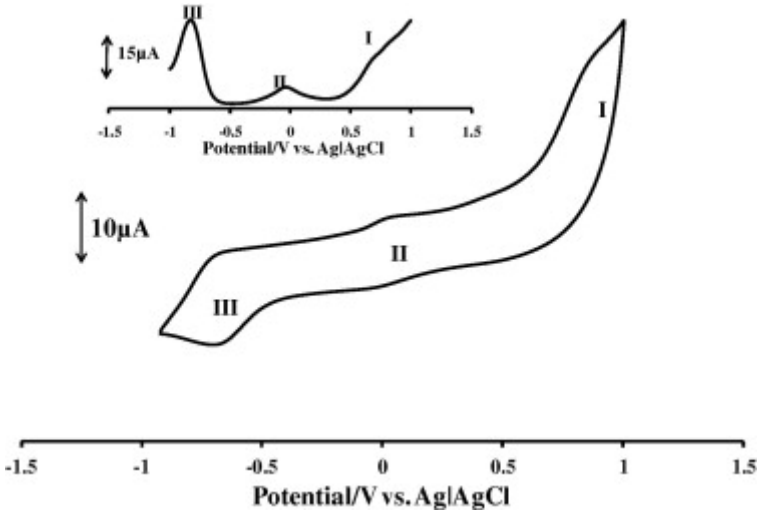

Fig. 5. Cyclic and square wave (inset) voltammograms of 10^{-3} M of complex 4 in distilled mixture of DCM and DMF containing 0.1 M $TBABF_4$. Scan rate: 100 mVs^{-1}.

3.1.3.3. Complex 5

The cyclic and square wave (inset) voltammetry profiles of ~1 × 10^{-3} M of complex 5, in freshly distilled DMF containing 0.1 M $TBABF_4$ as supporting electrolyte, are shown in Fig. 6. Wider potential window (−1.3–+1.3 V versus Ag|AgCl) was used compared to that used for complexes 3 and 4 (−1–+1 V versus Ag|AgCl), because ring-based processes were not observed for complex 5 within the latter potential window. Even though the UV–Vis spectra showed complex behavior, the cyclic voltammetry peaks were well resolved in Fig. 6. The cyclic voltammetry will be dominated by $Fe^{II}Pc$ derivatives since the spectrum of the complex showed this species to be dominant. Four distinct processes were observed. Process I (E_p = +0.87 V versus Ag|AgCl) was assigned to ring oxidation, $Fe^{III}Pc^{-1}/Fe^{III}Pc^{-2}$. This process

is irreversible as was the case for complexes 3 and 4. Process II ($E_{1/2}$ = +0.26 V versus Ag|AgCl) was assigned to metal oxidation, $Fe^{III}Pc^{-2}/Fe^{II}Pc^{-2}$, in comparison with other alkyl or aryl thio substituted FePc complexes [26], Table 1. Process II, with a weak cathodic component compared to the anodic component, was quasi-reversible. Process III ($E_{1/2}$ = −0.35 V versus Ag|AgCl) was assigned to metal reduction, $Fe^{II}Pc^{-2}/Fe^{I}Pc^{-2}$. This process was reversible, with peak separation, ΔE, of 60 mV versus Ag|AgCl, and cathodic to anodic current ratio of near unity. Process IV ($E_{1/2}$ = −0.96 V versus Ag|AgCl) was assigned to ring reduction, $Fe^{I}Pc^{-2}/Fe^{I}Pc^{-3}$.This process was quasi-reversible, with cathodic to anodic current ratio of near unity and peak separation, ΔE, of 120 mV versus Ag|AgCl compared to 91 mV for ferrocene at the same scan rate, 100 mV versus Ag|AgCl.

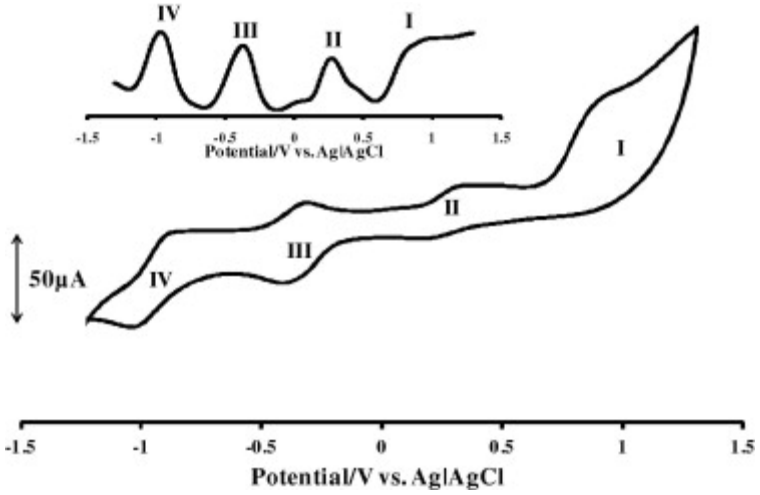

Fig. 6. Cyclic and square wave (inset) voltammograms of 10^{-3} M of complex 5 in freshly distilled DMF containing 0.1 M $TBABF_4$. Scan rate: 100 mVs^{-1}.

Due to the presence of more than one species in solution, spectroelectrochemical studies were not successful in the assignment of the cyclic voltammetry peaks. However, the assignments were based on the well known electrochemistry of FePc complexes in comparison with FePc complexes substituted with alkylthio groups, Table 1.

3.1.3.4. Complex 6

The synthesis of the cobalt analogue of complexes 3, 4 and 5 has been reported before [4], but it's electrochemical and spectroelectrochemical properties were not reported, hence they are reported in the current work, for the purpose of comparison with that of the new complexes. Fig. 7 shows both the cyclic and square wave (inset) voltammograms of ~1 × 10^{-3}M of complex 6 in freshly distilled DMF containing 0.1 M $TBABF_4$. A wider potential range (−2.0–+1.0 V) was used, compared to the other complexes, in order to observe the ring reduction processes. In coordinating solvents such as DMF, Co^{III}/Co^{II} couple occurs before the ring oxidation in CoPc complexes [27], thus process I (at 0.8 V) may be assigned to this process, but complicated by contribution from the oxidation of ring substituent as was the case for the rest of the complexes. The process occurs at more positive potential values compared to CoPc complexes in general, but is within the range of some arylthio substituted CoPc derivatives [28] and [29], Table 1.

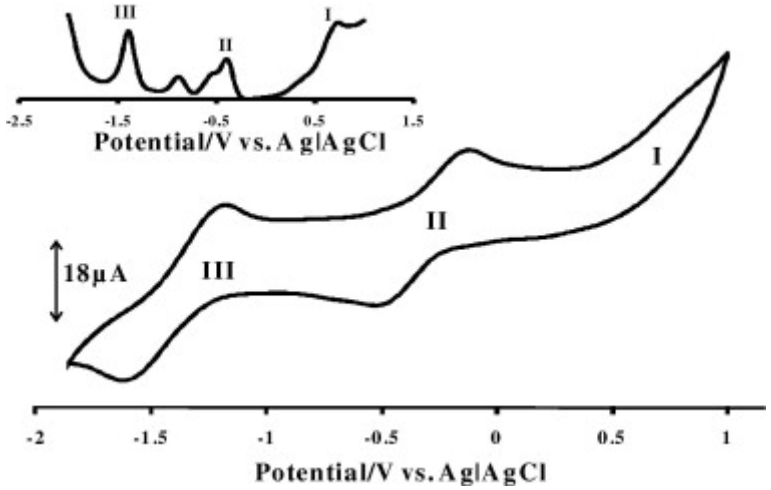

Fig. 7. Cyclic and square wave (inset) voltammograms of 10^{-3} M of complex 6 in freshly distilled DMF containing 0.1 M $TBABF_4$. Scan rate: 100 mVs^{-1}.

Processes II ($E_{1/2}$ = −0.32 V versus Ag|AgCl) and III ($E_{1/2}$ = −1.4 V versus Ag|AgCl) were quasi-reversible. Process II is in the potential range for $Co^{II}Pc^{2-}/Co^{I}Pc^{2-}$ species, while process III is typical of $Co^{I}Pc^{2-}/Co^{I}Pc^{3-}$ [27], Table 1. The more sensitive square wave voltammogram showed the presence of another process (−0.9 V). This was not observed on the cyclic voltammogram. The origin of the peak is not clear at the moment.

Spectroelectrochemical studies were used to confirm some of the assigned processes. The spectral changes in Fig. 8a were observed on the application of the potential of process II. The starting spectrum (curve i) shows considerable aggregation as a result of the high concentration used for the OTTLE cell. The peaks at 692 and 655 nm are associated with monomer and dimer respectively. A red-shift in the position of the Q-band, from 692 to 726 nm, was observed on the application of the potential of process II. There was an emergence of a new peak at 492 nm with increased intensity. New intense peak between 400 to 500 nm are characteristic of $Co^{I}Pc$ species [10]. The shift in Q-band without decrease in intensity is characteristic of metal-based reduction in MPc complexes. Thus spectral changes shown in Fig. 8a confirmed that couple II was as a result of the reduction of $Co^{II}Pc$ to $Co^{I}Pc$ (the number of moles of electrons transferred, n, was calculated to be approximately 1, using Eq. (1)). Also, distinct isobestic points at 580 and 710 nm showed that the process is a clear reduction involving two species. Application of the potential of process III resulted in the spectral changes shown in Fig. 8b. The starting spectrum (curve i), which is the last spectrum in Fig. 8a, has peaks at 726, 663, 492 and 604 nm. The peaks at 726 and 663 nm decrease in intensity without change in positions, while that at 492 nm shifted to 496 nm. The decrease in the intensity of Q-band is typical of ring-based process in MPcs. Bands in the 500 to 600 nm region are characteristic of ring-based reduction and the formation of a Pc^{3-} species [24]. Hence, reduction at potential of couple III resulted in the formation of $Co^{I}Pc^{3-}$ species.

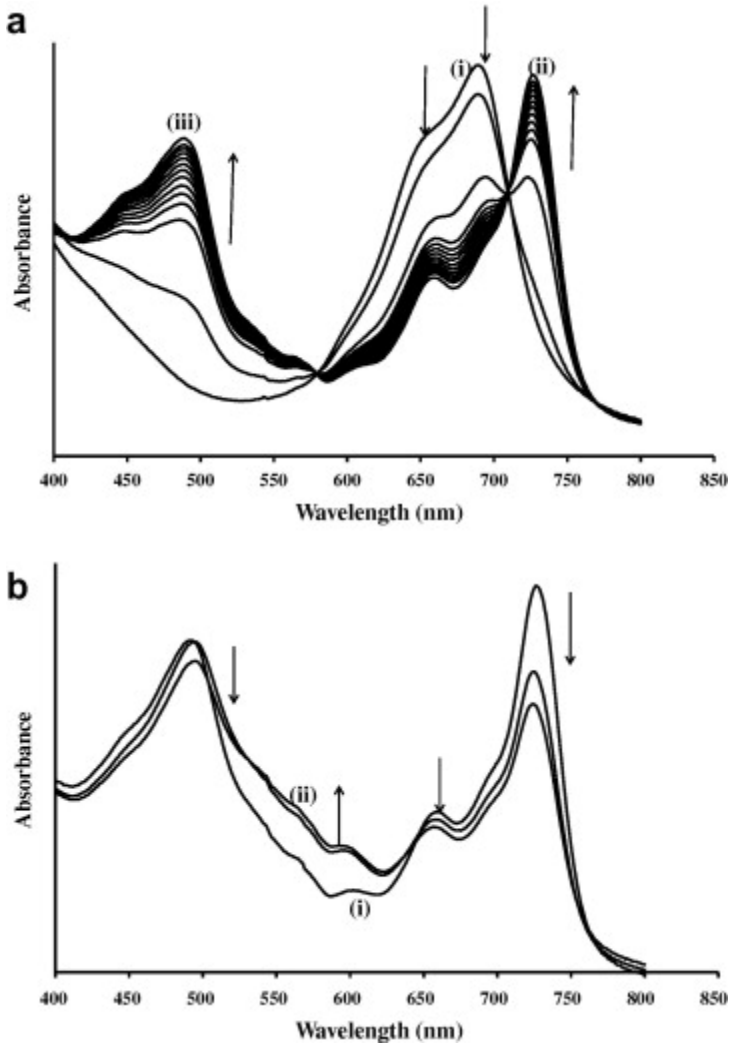

Fig. 8. UV–Vis spectral changes observed for complex 6 during controlled potential electrolysis at (a) −0.32 V (process II), (b) −1.40 V (process III). (i) Spectrum before electrolysis and (ii) spectrum after electrolysis. Electrolyte = DMF containing 0.1 M $TBABF_4$. The final spectrum in (a) is the starting spectrum in (b).

. Conclusions

The syntheses, spectroscopic and electrochemical properties of the new complexes: manganese (3), nickel (4) and iron (5) octakis-(2-diethylaminoethanethiol) phthalocyanines are reported. The observed spectroscopic and electrochemical properties of the complexes were distinctly defined by the nature of the central metals. During spectroelectrochemical studies, the UV–Vis spectra of complex 3 in DMF showed

bands characteristic of μ-oxo complex in MnPc complexes and that associated with the monomeric species. Well defined redox processes, assigned to $Mn^{III}Pc^{-2}/M^{II}Pc^{-2}$ and $Mn^{II}Pc^{-2}/M^{II}Pc^{-3}$ species, were observed and confirmed using spectroelectrochemical studies. Complex 4 showed aggregation behavior, characteristic of NiPc complexes, in THF. Complex 5 showed spectral property characteristic of stacked monomer in FePc. Solution electrochemistry of complex 5 showed four distinct redox processes, assigned to $Fe^{III}Pc^{-2}/Fe^{II}Pc^{-2}$, $Fe^{III}Pc^{-1}/Fe^{III}Pc^{-2}$, $Fe^{II}Pc^{-2}/Fe^{I}Pc^{-2}$ and $Fe^{I}Pc^{-2}/Fe^{I}Pc^{-3}$. Solution electrochemistry of the cobalt derivative (6) showed redox processes characteristic of $Co^{II}Pc^{-2}/Co^{I}Pc^{-2}$ and $Co^{I}Pc^{-2}/Co^{I}Pc^{-3}$ species.

Acknowledgements

This work was supported by the Department of Science and Technology (DST) and National Research Foundation (NRF) of South Africa through DST/NRF South African Research Chairs Initiative for Professor of Medicinal Chemistry and Nanotechnology and Rhodes University.

References

[1] C.C. Leznoff, A.B.P. Lever, Phthalocyanines Properties and Applications, vols. 1– 4, Weinheim, VCH, 1989–1996.

[2] N.B. Mckeown, in: Phthalocyanine Materials, Cambridge University Press, 1998.

[3] M. Idowu, T. Nyokong, Polyhedron 28 (2009) 416.

[4] Z.A. Bayur, Dyes Pigm. 65 (2005) 235.

[5] N. Sehlotho, M. Durmus_, V. Ahsen, T. Nyokong, Inorg. Chem. Commun. 11 (2008) 479.

[6] J. Zhu, F. Gu, J. Zhag, Mater. Lett. 61 (2007) 1296.

[7] W. Posiuk-Bronikoswska, M. Krajewska, I. Pfis-Kabulska, Polyhedron 18 (1998) 561.

[8] S. Knecht, K. DÜrr, G. Schmid, L.R. Subramanian, M. Hanack, J. Porphyr. Phthalocyan. 3 (1999) 292.

[9] D.K. Rittenberg, L. Baarrs-Hibbe, A. Böhm, J.S. Miller, J. Mater. Chem. 10 (2000) 241.

[10] M.J. Stillman, T. Nyokong, in: C.C. Leznoff, A.B.P. Lever (Eds.), Phthalocyanines: Properties and Applications, vol. 1, VCH, New York, 1989 (Chapter 3).

[11] P. Tau, T. Nyokong, Dalton Trans. (2006) 4482.

[12] G. Mbambisa, P. Tau, E. Antunes, T. Nyokong, Polyhedron 26 (2007) 5355.

[13] G. Mbambisa, T. Nyokong, Polyhedron 27 (2008) 2799.

[14] A.R. Ozkaya, A.G. Gurek, A. Gul, O. Bekaroglu, Polyhedron 16 (1997) 1877.

[15] K. Takahashi, M. Kawashima, Y. Tomita, M. Itoh, Inorg. Chim. Acta 232 (1995) 69.

[16] P. Tau, T. Nyokong, Electrochim. Acta 52 (2007) 4547.

[17] N.B. McKeown, in: K.M. Kadish, K.M. Smith, R. Guilard(Eds.), Porphyrin Handbook, Phthalocyanine Properties and Materials, vol. 15, 2003, Academic Press, New York (Chapter 98).

[18] J. Obirai, N. Pereira Rodrigues, F. Bedioui, T. Nyokong, J. Porphyr. Phthalocyan. 7 (2003) 508.

[19] A. Hadasch, A. Sorokin, A. Rabion, B. Meunier, New J. Chem. 22 (1998) 45.

[20] N. Grootboom, T. Nyokong, J. Mol. Cat. A: Chem. 179 (2002) 113.

[21] B. Agboola, K. Ozoemena, P. Westbroek, T. Nyokong, Electrochim. Acta 52 (2007) 2520.

[22] J. Janczak, R. Kubiak, M. S´ledz´ , H. Borrmann, Y. Grin, Polyhedron 22 (2003) 2689.

[23] J. Obirai, T. Nyokong, Electrochim. Acta 50 (2005) 3296.

[24] M.J. Stillman, in: C.C. Leznoff, A.B.P. Lever (Eds.), Phthalocyanines: Properties and Applications, vol. 3, VCH Publishers, New York, 1993 (Chapter 5).

[25] C.C. Leznoff, L.S. Black, A. Heibert, P.W. Causey, D. Christendat, A.B.P. Lever, Inorg. Chim. Acta 359 (2006) 2690.

[26] B.O. Agboola, K.I. Ozoemena, T. Nyokong, Electrochim. Acta 51 (2006) 4379.

[27] A.B.P. Lever, E.R. Milaeva, G. Speier, in: C.C. Leznoff, A.B.P. Lever (Eds.), Phthalocyanines: Properties and Applications, vol. 3, VCH Publishers, New York, 1993, p. 1.

[28] B. Agboola, K. Ozoemena, T. Nyokong, Electrochim. Acta 51 (2006) 4379.

[29] F. Matemadomboa, M.D. Maree, K.I. Ozoemena, P. Westbroek, J. Porphyr. Phthalocyan. 9 (2005) 484.